Noncausal Modeling and Closed-Loop Optimal Input Design for Cross-Directional Processes of Paper Machines

Qiugang Lu[1], Lee D. Rippon[1], R. Bhushan Gopaluni[1], Michael G. Forbes[2], Philip D. Loewen[3], Johan Backström[2], and Guy A. Dumont[4]

***Abstract*— We propose to use noncausal transfer functions to model the spatial behavior of cross-directional (CD) processes so as to circumvent the high-dimensionality of a causal transfer function. This noncausal representation is shown to have a causal-equivalent form. We prove that the covariance of maximum likelihood estimate of the causal-equivalent model asymptotically converges to that of the noncausal model. This result is then used to design optimal inputs in closed-loop for the original noncausal model of the CD process. An illustrative example is provided to highlight the advantage of using optimally designed excitation signal for CD closed-loop identification over white noise excitation or the current industrial practice of spatial bump excitation.**

I. INTRODUCTION

The cross-directional (CD) process of a paper machine refers to the direction perpendicular to the movement of paper sheet. It is a large-scale process involving hundreds of actuators and measurement bins, which brings significant challenges to the relevant CD system identification and controller design [1]. A popular control strategy employed on the CD process is model predictive control (MPC) that requires a high-quality process model. However, operation conditions of paper machines may vary over time due to factors such as grade change, and in such situations the initial process model may no longer be suitable to represent the underlying system dynamics [2]. As a result, the MPC performance often deteriorates. Thus once the quality of employed process model degrades we need to initiate an identification experiment to update the process model, preferably in the closed-loop for the sake of normal operation of paper machines [3], [4].

In terms of system identification, whether open-loop or closed-loop, it is well-known that a good excitation signal is necessary to attain a reliable and precise model [6]. Thus designing the excitation signal in an optimal way has received extensive attention in the last few decades. A number of well-known strategies have been proposed on this topic [7], [8]. More recent advances include using graph theory to address the input design problem for closed-loop MPC systems in time domain with probabilistic bound constraints on input and output [9], [10]. With regard to optimal input design of multi-input-multi-output (MIMO) and ill-conditioned systems, classical results are referred to [11]–[14]. However, for the CD process, a high-dimensional MIMO and ill-conditioned process, most existing input design research focuses on the open-loop case, see [15]. The main drawback of open loop input design is the resultant production loss as normal operations of process risk being interrupted. Results on closed-loop optimal input design for CD processes are scarce, with the current industrial practice of using spatial-bump-temporal-PRBS signals as excitations for closed-loop identification (termed as "bump excitations" in this paper) [16].

In this work, we design excitation signals for closed-loop CD process with optimal input design techniques. In particular, we focus on input design for the steady-state CD process model, in light of the fact that most of the time the CD process operates at steady-state. The major challenge is in representing the closed-loop CD process with a parsimonious parametric model to avoid having to use high dimensional transfer function models. Inspired by [17], we propose to develop a scalar noncausal model for closed-loop CD process to solve this problem. Furthermore, we demonstrate that one can always find a causal model that is equivalent to the noncausal model in the sense of asymptotic output spectra. It is further shown that the maximum likelihood estimate and parameter covariance matrix of the causal-equivalent model converge to those of the noncausal model asymptotically with probability one. In this sense, the optimal excitation signal can then be designed based solely on the causal model.

II. CD PROCESSES AND THE STEADY-STATE MODEL

A. Open-loop Steady-state CD Process Model

Consider the following *square* CD process at steady-state

$$y_{ss} = G_{ss}u_{ss} + v_{ss}, \tag{1}$$

where $y_{ss} \in \mathbb{R}^m$ and $u_{ss} \in \mathbb{R}^m$ represent the steady-state controlled variable (CV) and manipulated variable (MV) profiles, respectively. We denote m as the number of measurement boxes along the cross direction. $v_{ss} \in \mathbb{R}^m$ is the steady-state output disturbance. $G_{ss} \in \mathbb{R}^{m\times m}$ is the steady-state gain matrix and it has circulant columns (Toeplitz-structured), where each column is indeed the sampled impulse response

[1]Qiugang Lu, Lee Rippon and Bhushan Gopaluni are with the Department of Chemical and Biological Engineering, The University of British Columbia, Vancouver, BC, Canada. Email: qglu@chbe.ubc.ca, leeripp@chbe.ubc.ca, bhushan.gopaluni@ubc.ca

[2]Michael Forbes and Johan Backström are with the Honeywell Process Solutions, 500 Brooksbank Ave, North Vancouver, BC, Canada. Email: michael.forbes@honeywell.com, johan.backstrom@honeywell.com

[3]Philip Loewen is with the Department of Mathematics, The University of British Columbia, Vancouver, BC, Canada. Email: loew@math.ubc.ca

[4]Guy Dumont is with the Department of Electrical and Computer Engineering, The University of British Columbia, Vancouver, BC, Canada. Email: guyd@ece.ubc.ca

of a single actuator along the CD at steady-state. We impose the following assumption on G_{ss} matrix.

Assumption 1: All actuators of the CD process have identical and symmetric impulse response coefficients in the spatial direction at steady-state. The columns of G_{ss} matrix are indeed sampled version of these responses.

We further re-write the spatial disturbance as $v_{ss} = \phi e_{ss}$, where e_{ss} is white noise in spatial direction and $\phi \in \mathbb{R}^{m\times m}$ is the steady-state noise model. For simplicity we assume that ϕ has a structure similar to that of G_{ss}.

B. Closed-loop Steady-state CD Process Model

Designing closed-loop dither signals requires an explicit expression of the controller in the formulation of input design objective function. It is well-known that CD MPC may display time-varying or even nonlinear dynamics if any constraint is active. Thus input design for closed-loop MPC systems involving active constraints is non-trivial. To simplify this problem we introduce the following assumption.

Assumption 2: The MPC is assumed to operate in a linear mode with no active constraints.

With Assumption 2, the closed expression of MPC is shown to be [3]

$$K_{ss} = -Q_3^{-1}\alpha_K G_{ss} Q_1, \tag{2}$$

where Q_1 is the weight matrix in MPC objective function penalizing the deviation of CV profile from its set-point. Q_3 is the corresponding weight matrix to penalize the offset of steady-state MV from its target. α_K is a constant determined from the dynamic model of actuators. In practice the weighting matrices Q_1 and Q_3 are often chosen to be diagonal. Assuming Q_1 and Q_3 to be diagonal, the controller K_{ss} then has a matrix structure similar to that of gain matrix G_{ss}. The structural similarity between K_{ss} and G_{ss} will be used in the derivations below.

Remark 1: While Assumption 2 seems to be a restrictive assumption in practical implementation of our algorithm, industrial experience reveals that a well-tuned CD MPC normally operates without active constraints. We stress that our method in this paper also works when Assumption 2 is relaxed to have a fixed active set, whereby the active constraint can be explicitly considered [5]. The extension to incorporate varying constraints will be our future work.

Combining (1) and (2), we can easily arrive at the following closed-loop CD process

$$\begin{aligned} y_{ss} &= (I+G_{ss}K_{ss})^{-1}G_{ss}K_{ss}r + (I+G_{ss}K_{ss})^{-1}v_{ss}, \quad (3)\\ u_{ss} &= (I+K_{ss}G_{ss})^{-1}r - (I+K_{ss}G_{ss})^{-1}K_{ss}v_{ss}, \quad (4)\end{aligned}$$

where $r \in \mathbb{R}^m$ is the spatial excitation signal to be designed.

C. Spatial Optimal Input Design for the CD Process

When it comes to spatial optimal input design, the parameters of interest here are those in the gain matrix G_{ss} (or more specifically, the parameters in a column of G_{ss}). However, optimal input design directly based on closed-loop model (3)-(4) is non-trival due to the large input-output dimensions as well as the large number of parameters in G_{ss}. To circumvent this problem, we propose to use a scalar transfer function along the spatial coordinate to represent the steady-state response of CD actuators. In this sense, the original optimal input design aimed for the MIMO CD model can be re-formulated into that for the scalar spatial model, which significantly reduces the complexity. However, the disadvantage is that this scalar spatial transfer function has to be noncausal to capture the responses of actuators on both sides (see Fig. 1), analogous to the 'past' and 'future' in the conventional time coordinate. We provide theoretical basis showing that the noncausal model can be further converted to a causal-equivalent model such that the input design can be performed based on this causal model.

III. Causal Scalar Transfer Function Representation of the CD Process

A. Noncausal Scalar Model of the Closed-loop CD Process

From the aforementioned structure (neglecting the asymmetric responses of actuators near the sheet edge) of G_{ss} as well as Assumption 1, one is readily able to extract a scalar noncausal finite impulse response (FIR) model from any single column of G_{ss} to represent the spatial impulse response of an actuator

$$g(\lambda,\lambda^{-1}) = g_{-n}\lambda^{-n} + \ldots + g_0 + \ldots + g_n\lambda^n, \tag{5}$$

where $n < m$ is a truncated index representing significant coefficients. The positive and negative powers of λ denote the anti-causal and causal shift. The $g_i,\ i = -n,\ldots,n$, are spatial impulse response coefficients and in general symmetry of these coefficients is enforced, i.e., $g_i = g_{-i}$. Since in most cases the noncausal FIR model (5) has a high order (i.e., n is large), a parsimonious noncausal transfer function is necessary to simplify this model. First, we present the following assumption.

Assumption 3: The complex trigonometric polynomial (5) has real and symmetric coefficients. Moreover, this polynomial is positive at any points on the unit circle $|\lambda| = 1$.

With this assumption it follows from the Fejér-Riesz Theorem that we can factorize $g(\lambda,\lambda^{-1})$ as

$$g_{-n}\lambda^{-n} + \ldots + g_0 + \ldots + g_n\lambda^n = M(\lambda)M(\lambda^{-1}),\ \forall\omega, \tag{6}$$

where $\lambda = e^{j\omega}$. Here $M(\lambda^{-1})$ has the following expression

$$M(\lambda^{-1}) = m_0 + m_1\lambda^{-1} + \ldots + m_n\lambda^{-n},$$

where $m_i, i = 1,\ldots,n$, are the coefficients. An immediate observation is that the frequency response of the left-hand side of (6) is real and non-negative at any frequency, which places certain restrictions on the scope of possible spatial impulse response shapes that we may investigate. However, industrial experience shows that most actual actuator response shapes are able to satisfy this condition. The relationship (2) affirms that if G_{ss} satisfies (6) then so does K_{ss}.

After obtaining the causal FIR model $M(\lambda^{-1})$, the next step would be to find a parsimonious transfer function model (e.g. output-error model) to represent $M(\lambda^{-1})$. This process can be accomplished from the system identification

toolbox in Matlab and the original noncausal $g(\lambda,\lambda^{-1})$ is approximated by $\bar{g}(\lambda,\lambda^{-1})$ as follows

$$\begin{aligned}\bar{g}(\lambda,\lambda^{-1}) &= \frac{B(\lambda)B(\lambda^{-1})}{A(\lambda)A(\lambda^{-1})}, &(7)\\ B(\lambda^{-1}) &= b_0+b_1\lambda^{-1}+\ldots+b_{n_b}\lambda^{-n_b}, &(8)\\ A(\lambda^{-1}) &= 1+a_1\lambda^{-1}+\ldots+a_{n_a}\lambda^{-n_a}, &(9)\end{aligned}$$

where n_a and n_b are the orders of $B(\lambda^{-1})$ and $A(\lambda^{-1})$, respectively. In a similar fashion, the noncausal transfer function form of the controller is assumed to be

$$\begin{aligned}\bar{k}(\lambda,\lambda^{-1}) &= \frac{F(\lambda)F(\lambda^{-1})}{E(\lambda)E(\lambda^{-1})}, &(10)\\ F(\lambda^{-1}) &= f_0+f_1\lambda^{-1}+\ldots+f_{n_f}\lambda^{-n_f}, &(11)\\ E(\lambda^{-1}) &= 1+e_1\lambda^{-1}+\ldots+e_{n_e}\lambda^{-n_e}, &(12)\end{aligned}$$

where n_e and n_f are the orders of $E(\lambda^{-1})$ and $F(\lambda^{-1})$, respectively. From (7)-(12), the original high-dimensional MIMO steady-state closed-loop model (3)-(4) can be replaced by scalar but noncausal transfer functions[1]

$$\begin{aligned}y(x) &= \frac{\bar{g}}{1+\bar{g}\bar{k}}r(x)+\frac{1}{1+\bar{g}\bar{k}}v(x), &(13)\\ u(x) &= \frac{1}{1+\bar{g}\bar{k}}r(x)-\frac{\bar{k}}{1+\bar{g}\bar{k}}v(x), &(14)\end{aligned}$$

where x stands for the spatial coordinate. Note that the input and output sensitivity functions have the same noncausal transfer function representation as shown above.

B. Causal Equivalent Closed-loop Models

The closed-loop scalar noncausal model of the CD process (13)-(14) is still not in a form convenient for traditional optimal input design algorithms. In this subsection we develop a method to find causal-equivalent models for the noncausal transfer functions such as $\bar{g}(\lambda,\lambda^{-1})$. First, the following Lemma is necessary.

Lemma 1: Suppose that $\bar{g}_1(\lambda,\lambda^{-1})$ and $\bar{g}_2(\lambda,\lambda^{-1})$ satisfy the conditions in Assumption 3. Then the sum $\bar{g}_1(\lambda,\lambda^{-1})+\bar{g}_2(\lambda,\lambda^{-1})$ also has a factorization as (6).

Proof: Since the conditions in Assumption 3 apply to polynomials $\bar{g}_1(\lambda,\lambda^{-1})$ and $\bar{g}_2(\lambda,\lambda^{-1})$, we have

$$\begin{aligned}\bar{g}_1(e^{j\omega},e^{-j\omega}) &\geq 0,\ \forall\omega,\\ \bar{g}_2(e^{j\omega},e^{-j\omega}) &\geq 0,\ \forall\omega,\end{aligned}$$

Thus it follows that

$$\bar{g}_1(e^{j\omega},e^{-j\omega})+\bar{g}_2(e^{j\omega},e^{-j\omega}) \geq 0,\ \forall\omega. \quad (15)$$

Besides, the coefficient sequence of (15) is real and symmetric. From the Fejér-Riesz Theorem there always exists an $M(\lambda)$ such that (6) is satisfied. ■

Defining $\bar{S}=\frac{1}{1+\bar{g}\bar{k}}$, from (13)-(14), we have

$$\bar{S}=\frac{A(\lambda)A(\lambda^{-1})E(\lambda)E(\lambda^{-1})}{A(\lambda)A(\lambda^{-1})E(\lambda)E(\lambda^{-1})+B(\lambda)B(\lambda^{-1})F(\lambda)F(\lambda^{-1})}. \quad (16)$$

[1]In the sequel, we will omit the subscript and use the argument x to indicate the steady-state input and output sequence.

From Lemma 1, it follows that the denominator of (16) can be factorized to be the product of a causal FIR filter and its anti-causal form. Therefore, the closed-loop transfer functions (13)-(14) can be simplified as

$$\begin{aligned}y(x) &= \bar{S}_1(\lambda,\lambda^{-1})r(x)+\bar{S}_2(\lambda,\lambda^{-1})v(x), &(17)\\ u(x) &= \bar{S}_2(\lambda,\lambda^{-1})r(x)-\bar{S}_3(\lambda,\lambda^{-1})v(x), &(18)\end{aligned}$$

where $\bar{S}_i(\lambda,\lambda^{-1}), i=1,2,3$, has a structure similar to that of (7) and (10). Further notice that ϕ can also be represented by a noncausal transfer function as is assumed in the previous sections. In other words, the spatial noise v_{ss} has the following expression

$$v(x)=\bar{h}(\lambda,\lambda^{-1})e(x)=\frac{D(\lambda)D(\lambda^{-1})}{C(\lambda)C(\lambda^{-1})}e(x), \quad (19)$$

where $\{e(x)\}$ is a spatial white noise sequence. To find a causal-equivalent transfer function for (17)-(19), we establish the following theorem.

Theorem 1: Consider a stochastic process with the output sequence $\{y(x),x=1,\ldots,m\}$ generated according to the following noncausal Box-Jenkins model

$$y(x)=\frac{M(\lambda)M(\lambda^{-1})}{N(\lambda)N(\lambda^{-1})}r(x)+\frac{R(\lambda)R(\lambda^{-1})}{S(\lambda)S(\lambda^{-1})}e(x), \quad (20)$$

where $\{e(x),x=1,\ldots,m\}$ is a Gaussian white noise sequence. The polynomials with arguments λ^{-1} and λ are the causal and anti-causal parts, respectively. Assume that all polynomials have no zeros on the unit circle and are minimum phase. Then there exist causal polynomials $\tilde{M}_y(\lambda^{-1})$, $\tilde{N}_y(\lambda^{-1})$, $\tilde{R}_y(\lambda^{-1})$, $\tilde{S}_y(\lambda^{-1})$ and a white noise sequence $\{\tilde{e}_y(x)\}$ as well as a stochastic sequence $\{\tilde{y}(x)\}$ which has the same spectra as $\{y(x)\}$ such that,

$$\tilde{y}(x)=\frac{\tilde{M}_y(\lambda^{-1})}{\tilde{N}_y(\lambda^{-1})}r(x)+\frac{\tilde{R}_y(\lambda^{-1})}{\tilde{S}_y(\lambda^{-1})}\tilde{e}_y(x). \quad (21)$$

Proof: Multiplying both sides of (20) by using $N(\lambda)N(\lambda^{-1})S(\lambda)S(\lambda^{-1})$, we obtain

$$\begin{aligned}N(\lambda)N(\lambda^{-1})S(\lambda^{-1})S(\lambda)y(x)=M(\lambda)M(\lambda^{-1})S(\lambda)\\ S(\lambda^{-1})r(x)+N(\lambda)N(\lambda^{-1})R(\lambda)R(\lambda^{-1})e(x).\end{aligned} \quad (22)$$

Define the roots of causal polynomials $M(\lambda^{-1})$, $N(\lambda^{-1})$, $R(\lambda^{-1})$, $S(\lambda^{-1})$ to be, respectively, α_i, β_i, γ_i and δ_i. Let

$$\begin{aligned}\pi_M=\prod_i\frac{\lambda^{-1}-\alpha_i}{\lambda-\alpha_i},\ \pi_N=\prod_i\frac{\lambda^{-1}-\beta_i}{\lambda-\beta_i},\\ \pi_R=\prod_i\frac{\lambda^{-1}-\gamma_i}{\lambda-\gamma_i},\ \pi_S=\prod_i\frac{\lambda^{-1}-\delta_i}{\lambda-\delta_i}.\end{aligned}$$

Notice that $N(\lambda)N(\lambda^{-1})\pi_N=N^2(\lambda^{-1})$ and the same also holds for $M(\lambda)$, $R(\lambda)$, and $S(\lambda)$. Multiplying both sides of (22) by $\pi_M\pi_S$, after some manipulations, we have

$$\begin{aligned}N^2(\lambda^{-1})S^2(\lambda^{-1})\tilde{y}(x)=\\ M^2(\lambda^{-1})S^2(\lambda^{-1})r(x)+R^2(\lambda^{-1})\tilde{e}_y(x),\end{aligned} \quad (23)$$

where $\tilde{y}(x)=\frac{\pi_M}{\pi_N}y(x)$, $\tilde{e}_y(x)=\frac{\pi_M\pi_S}{\pi_N\pi_R}e(x)$. Since π_M, π_N, π_R and π_S are all-pass filters, $\{\tilde{e}_y(x)\}$ is a Gaussian white noise

sequence with the same spectra as $\{e(x)\}$ but may correspond to different realizations. Besides, $\{\tilde{y}(x)\}$ has the same spectra as $\{y(x)\}$. Therefore, (21) is verified by pairing $\tilde{M}(\lambda^{-1}) = M^2(\lambda^{-1})$ and so on with (23). ■

Remark 2: From Theorem 1 one may interpret the equivalence between $\{\tilde{y}(x)\}$ and $\{y(x)\}$ in terms of the spectra, although realizations might be different. However, this equivalence greatly facilitates the maximum likelihood estimation for the original noncausal model by reducing it into a causal-equivalent form. The rationale for performing identification in this manner has been explained in [17] for an ARX model. The conclusion is that the log-likelihood function of the noncausal model converges to that of the causal model with probability one as the sample number tends to infinity. This result can also be extended to the noncausal Box-Jenkins model in (20).

Similarly, the input signal $u(x)$ in (18) can also be represented through causal filters

$$\tilde{u}(x) = \frac{\tilde{M}_u(\lambda^{-1})}{\tilde{N}_u(\lambda^{-1})} r(x) + \frac{\tilde{R}_u(\lambda^{-1})}{\tilde{S}_u(\lambda^{-1})} \tilde{e}_u(x), \tag{24}$$

where $\{\tilde{u}(x)\}$ and $\{u(x)\}$ have the same spectra. The equations (21) and (24) are necessary for the optimal input design in the sequel.

C. Covariance Matrix Equivalence of the Causal and Noncausal Model Parameter Estimates

It is well-known that if the white noise is Gaussian distributed, the prediction error method with properly chosen criterion coincides with the maximum likelihood estimation. In [17], it is shown that the log-likelihood function of the noncausal ARX model and that of the corresponding causal ARX model converge to the same value as the sample number tends to infinity. In this subsection we will demonstrate a similar statement for closed-loop data.

Theorem 2: Consider the following noncausal process model (θ is the parameter in a compact set Ω)

$$y(x) = \bar{g}(\lambda, \lambda^{-1}, \theta) u(x) + \bar{h}(\lambda, \lambda^{-1}, \theta) e(x), \tag{25}$$

where $\bar{g}$ is defined in (7)-(9) and $\bar{h}$ is defined in (19). $e(x)$ is Gaussian white noise. Suppose that the data is generated in closed-loop with controller (10)-(12) and that all relevant transfer functions are uniformly stable. Denote $\mathscr{L}_y^m(y)$ as the log-likelihood function of the noncausal model (25) and $\mathscr{L}_{\tilde{y}}^m(\tilde{y})$ as the log-likelihood function of the causal-equivalent model of (25) obtained similarly as (21). Then, as $m \to \infty$ (m is the spatial sample number, i.e., the number of measurement bins),

$$\sup_{\theta \in \Omega} |\mathscr{L}_y^m(y) - \mathscr{L}_{\tilde{y}}^m(\tilde{y})| \xrightarrow{\text{w.p.1}} 0, \tag{26}$$

$$\sup_{\theta \in \Omega} \left\| \frac{d\mathscr{L}_y^m(y)}{d\theta} - \frac{d\mathscr{L}_{\tilde{y}}^m(\tilde{y})}{d\theta} \right\| \xrightarrow{\text{w.p.1}} 0. \tag{27}$$

Proof: The proof of (26) follows along Proposition 3 in [17] and the proof for (27) is shown in Appendix. ■

Remark 3: Theorem 2 implies that both the log-likelihood function and its derivative with respect to the parameter θ obtained from the noncausal and causal-equivalent models are identical asymptotically. Therefore, we can conclude that the parameter covariances from these two schemes coincide, and hence we may perform the optimal input design based solely on the causal-equivalent model.

IV. Closed-loop Optimal Input Design

In this section closed-loop optimal input design for the steady-state CD process is investigated. As mentioned above we can accomplish this task with the causal-equivalent representation of CD process. Note that in practice the noise model parameters are of less interest and thus we split the parameter θ as $\theta = [\rho^T \ \eta^T]^T$, where ρ is the process model parameter and η is the noise model parameter. For optimal input design our objective is minimizing the covariance of ρ by selecting the optimal excitation signal. From Theorem 2 the parameter covariance of ρ, P_ρ, is expressed as

$$P_\rho \sim \frac{1}{m} \left[\frac{1}{2\pi\lambda_0} \int_{-\pi}^{\pi} \frac{1}{|\tilde{h}(e^{j\omega}, \eta_0)|^2} \frac{\partial \tilde{g}(e^{j\omega}, \rho_0)}{\partial \rho} \Phi_{\tilde{u}}(\omega) \frac{\partial \tilde{g}^T(e^{-j\omega}, \rho_0)}{\partial \rho} d\omega \right]^{-1}, \tag{28}$$

where λ_0 is the variance of noise $\tilde{e}_y(x)$. $\tilde{g}$ and $\tilde{h}$ are the causal equivalent forms of $\bar{g}$ and $\bar{h}$, respectively. The input spectrum $\Phi_{\tilde{u}}(\omega)$, according to (24), is related to the excitation spectrum $\Phi_r(\omega)$ via

$$\Phi_{\tilde{u}}(\omega) = \left| \frac{\tilde{M}_u(e^{-j\omega})}{\tilde{N}_u(e^{-j\omega})} \right|^2 \Phi_r(\omega) + \left| \frac{\tilde{R}_u(e^{-j\omega})}{\tilde{S}_u(e^{-j\omega})} \right|^2 \lambda_0. \tag{29}$$

The closed-loop optimal input design can be formulated as minimizing a function of the parameter covariance P_ρ subject to a set of constraints, e.g., input and output power constraints,

$$\min_{\Phi_r(\omega)} \quad f_0(P_\rho(\Phi_r(\omega))) \tag{30}$$

$$s.t. \quad \frac{1}{2\pi} \int_{-\pi}^{\pi} \Phi_u(\omega) d\omega \le c_u, \tag{31}$$

$$\frac{1}{2\pi} \int_{-\pi}^{\pi} \Phi_y(\omega) d\omega \le c_y, \tag{32}$$

where c_u and c_y are the power limits on input and output signals. The constraints (31)-(32) can be written in terms of the design variable $\Phi_r(\omega)$ by (29) and (21), respectively. As this optimization problem is still infinite-dimensional (since $\Phi_r(\omega)$ is a continuous function of ω), a technique known as finite dimensional parameterization [18] can be employed to reduce it into finite-dimensional. Specifically, $\Phi_r(\omega)$ can be parameterized by the definition of a spectrum

$$\Phi_r(\omega) = \sum_{k=-m_c}^{m_c} c_k e^{-j\omega k} \ge 0, \quad \forall \omega, \tag{33}$$

where c_k, $k = -m_c, \ldots, m_c$, are the parameters, and m_c is the selected number of parameters. With (33) the original optimization problem can be cast into one with finite number of parameters. Note that the non-negativity constraint on the parameterized spectrum (33) at any frequency has to be satisfied while searching for the optimal c_k. This requirement

can be fulfilled by using the KYP lemma and constructing a controllable and observable state-space realization for the spectrum [18]. After these modifications the resulting optimization problem is convex (choose $f_0(\cdot)$ to be convex) and can be readily solved by off-the-shelf solvers such as the CVX toolbox.

Remark 4: Note that the aforementioned optimal input design only considers the power constraints on the input and output (31)-(32). However, in practice, the hard constraints on CVs and MVs make more sense and this is still an open problem for frequency-domain optimal input design. Besides, specific to the CD process, the second-order bending constraints preventing 'picketing' on actuators are also important. These practical constraints are beyond the scope of this paper and will be investigated in future work.

Remark 5: A common issue for optimal input design is that the covariance matrix depends on the true parameter values, as shown in (28), which may be unaccessible in practice. One remedy is the adaptive input design scheme: specifying an initial parameter value to design an optimal input signal, updating parameter estimates via identifications and using the updated parameter value to design a new optimal input. This process iterates until it converges.

V. Case Study

In this section we use a simulation example to validate the proposed CD process modeling and closed-loop optimal input design methods. In particular, we would compare the effect of optimally designed input on parameter estimates with that of bump excitation signal that is currently employed in the industry [16].

In practice, the spatial response shape of a single actuator is a nonlinear function [3] with four parameters $\gamma, \xi, \beta, \alpha$, representing the gain, width, divergence and attenuation, respectively. In this example, these parameters are specified with values, respectively, $\gamma = 0.3802$, $\xi = 268.6414$ *mm*, $\beta = 0.10$, $\alpha = 3.5$. The response shape under impulse signal of amplitude 5 is illustrated as the red curve (upper plot) in Fig. 1. The CD process has 222 actuators and measurement bins. The controller is chosen to be CD-MPC with prediction horizon 25 samples and control horizon 5 samples (sampling interval is 12 seconds). We choose weighting matrices in the cost function as $Q_1 = 0.4I$ and $Q_3 = 0.1667I$. The parameter α_K in (2) is computed to be 12.3212. From Section III one is able to obtain noncausal scalar models for the CD process and the controller, respectively. The impulse response curves of these noncausal models are shown in Fig. 1 in the blue dash-dotted curves. Note that for simplicity we have chosen $n_b = n_f = 1$, $n_a = n_e = 2$. Higher order models improve the quality of estimates but also increase the computational cost in designing the optimal input. The noise variance is chosen to be 0.1 with noise model $\phi = I$ (output-error structure). Fig. 2 shows the optimal spectrum based on causal-equivalent models with $c_u = 50$. Notice that small process gain (the causal-equivalent model has even smaller gain) as in this case requires a large excitation signal to achieve a good signal-to-noise ratio.

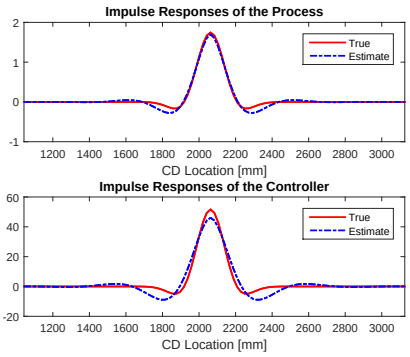

Fig. 1. The impulse response of a single actuator (red solid line) and the impulse response of the estimated noncausal transfer function (blue dash-dotted line).

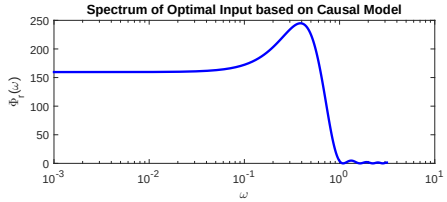

Fig. 2. Spectrum of the optimal input based on causal-equivalent model of the CD process.

To make a fair comparison between the optimal and bump excitations, we set a hard constraint ± 10 on the amplitude of excitation signals. For the optimally designed input, if any part of its amplitude violates this constraint, we set that part at the corresponding bound. For the bumped signal, the amplitudes of bumps alternate between -10 and 10. In order to further show the optimality of designed input, we generate another excitation signal that is a white noise sequence with the *same* variance as the optimal input. For each excitation signal we perform 100 Monte-Carlo simulations and a process model is identified in each simulation. Fig. 3 shows the impulse responses of estimated models under these three excitation signals. One can see that estimates under the optimal input have the smallest variance while estimates under the bumped signal show the largest variance. Specifically, the averaged errors of estimated impulse responses relative to the true response are shown to be 0.0643, 1.3344 and 0.4479, respectively, for the optimal input, bumped input and white noise input. Thus our optimal input outperforms the bump excitation signal and white noise signal (with the same variance) in terms of the identification performance.

VI. Summary

We developed an approach to represent the closed-loop steady-state CD process model with noncausal scalar transfer functions. The advantage of using noncausal models is that it circumvents the problem of large dimensions associated with MIMO representations of CD processes. We then show that these noncausal transfer functions can be further represented by spectrally equivalent causal transfer functions. A closed-loop optimal input design framework is proposed based on

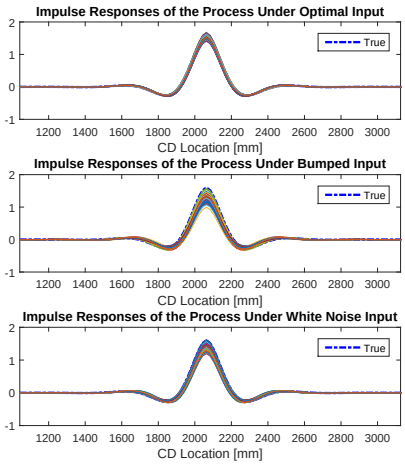

Fig. 3. The impulse responses of the estimated process model in the closed-loop under the optimally designed input (upper plot), the bumped input (middle plot), and the white noise input (bottom plot) in 100 Monte-Carlo simulations.

these causal-equivalent models. An example is provided to validate the proposed approaches and demonstrate the advantage of optimal input in system identification performance over the industrial practice of using bump excitation as well as white noise excitation.

APPENDIX

We outline the proof for (27) in Theorem 2. First the following lemma is necessary.

Lemma 2: Consider a set of uniformly stable *causal or noncausal* filters $G(\lambda,\theta),\theta\in\Omega$, and $H(\lambda,\theta),\theta\in\Omega$. Define $u(x),\ x=1,\ldots,m$, as a bounded signal sequence, and $e(x),\ x=1,\ldots,m$, as a sequence of Gaussian white noise with zero mean and variance σ^2. The signal $s(x),\ x=1,\ldots,m$, is generated via

$$s_\theta(x)=G(\lambda,\theta)u(x)+H(\lambda,\theta)e(x). \tag{34}$$

Then as $m\to\infty$, the sample variance of $s_x(\theta)$ converges *uniformly* in probability to the ensemble variance

$$\sup_{\theta\in\Omega}\left\|\frac{1}{m}\sum_{x=1}^{m}s_\theta(x)s_\theta^T(x)-\frac{1}{m}\sum_{x=1}^{m}\mathbb{E}s_\theta(x)s_\theta^T(x)\right\|\to 0,\text{w.p.1}. \tag{35}$$

Note that (35) is an extension of Theorem 2B.1 in [6] to noncausal models. The proof follows a similar line and is thus omitted here. Based on Lemma 2, as $m\to\infty$, the following statements hold

- $\frac{d\mathscr{L}_y^m(y,\theta)}{d\theta}$ converges uniformly w.r.t. θ w.p.1;
- $\frac{d\mathscr{L}_{\tilde{y}}^m(\tilde{y},\theta)}{d\theta}$ converges uniformly w.r.t. θ w.p.1.

The reason is that both $\frac{d\mathscr{L}_y^m(y)}{d\theta}$ and $\frac{\mathscr{L}_{\tilde{y}}^m(\tilde{y},\theta)}{d\theta}$ can similarly be considered as generated from uniformly stable filters. Thus from Lemma 2 the above statements hold. On the other hand, from the proof of (26) in [17], one can see that both $\mathscr{L}_y^m(y)$ and $\mathscr{L}_{\tilde{y}}^m(\tilde{y},\theta)$ converge uniformly to the same value, denoted as $\sigma^2(\theta)$. Based on Theorem 7.17 in [19], with the above statements, we have, as $m\to\infty$,

$$\sup_{\theta\in\Omega}\left\|\frac{d\mathscr{L}_y^m(y,\theta)}{d\theta}-\frac{d\sigma^2(\theta)}{d\theta}\right\|\to 0,\ \text{w.p.1}, \tag{36}$$

$$\sup_{\theta\in\Omega}\left\|\frac{d\mathscr{L}_{\tilde{y}}^m(\tilde{y},\theta)}{d\theta}-\frac{d\sigma^2(\theta)}{d\theta}\right\|\to 0,\ \text{w.p.1}. \tag{37}$$

From the Triangle Inequality, the result (27) follows. It should be pointed out that in this proof the 'uniformity' of the convergence in probability is a necessary condition for the results to hold.

REFERENCES

[1] R.M. Morales and W.P. Heath, "The robustness and design of constrained cross-directional control via integral quadratic constraints," *IEEE Control Syst. Technol.*, 19(6):1421–1432, 2011.

[2] Q. Lu, M. Forbes, B. Gopaluni, P. Loewen, J. Backström and G. Dumont, "Performance assessment of cross-directional control for paper machine," *IEEE Control Syst. Technol.*, 25(1): 208–221, 2017.

[3] J. Fan. *Model Predictive Control for Multiple Cross-directional Processes: Analysis, Tuning, and Implementation*. PhD thesis, The University of British Columbia, Canada, 2003.

[4] T.A.N. Heirung, B. Foss and B.E. Ydstie, "MPC-based dual control with online experiment design," *J. Process Control*, 32: 64–76, 2015.

[5] S. Wang, J.M. Simkoff, M. Baldea, L.H. Chiang, I. Castillo, R. Bindlish and D.B. Stanley, "Data-driven plant-model mismatch quantification in input-constrained linear MPC," In 11^{th} *IFAC DYCOPS-CAB*, Trondheim, Norway, 2016.

[6] L. Ljung. *System Identification: Theory for the User*. Englewood Cliffs, New Jersey: Prentice-Hall, Inc., 1999.

[7] R. Hildebrand, M. Gevers, and G.E. Solari, "Closed-loop optimal experiment design: Solution via moment extension," *IEEE Autom. Control*, 60(7):1731–1744, 2015.

[8] C.A. Larsson, A. Ebadat, C.R. Rojas, X. Bombois, and H. Hjalmarsson, "An application-oriented approach to dual control with excitation for closed-loop identification," *Eur. J. Control*, 29(5): 1–16, 2016.

[9] Afrooz Ebadat, *On Application Oriented Experiment Design for Closed-loop System Identification*, PhD Thesis, Kungliga Tekniska Högskolan, Sweden, 2015.

[10] P.E. Valenzuela, , R.R. Cristian, and H. Hjalmarsson, "A graph theoretical approach to input design for identification of nonlinear dynamical models," *Automatica*, 51(1): 233-242, 2015.

[11] Y. Zhu and P. Stec, "Simple control-relevant identification test methods for a class of ill-conditioned processes," *J. Process Control*, 16(10): 1113-1120, 2006.

[12] O. Vaillant, A. Kuramoto, and C. Garcia, "Effectiveness of signal excitation design methods for identification of ill-conditioned and highly interactive processes," *Ind. Eng. Chem. Res.*, 52(14): 5120-5135, 2013.

[13] M.L. Darby and M. Nikolaou, "Identification test design for multivariable model-based control: An industrial perspective," *Control Eng. Pract.*, 22(1): 165-180, 2014.

[14] A. Micchi and G. Pannocchia, "Comparison of input signals in subspace identification of multivariable ill-conditioned systems," *J. Process Control*, 18(6): 582-593, 2008.

[15] K.K. Kim and R.D. Braatz, "Convex relaxation of sequential optimal input design for a class of structured large-scale systems: process gain estimation," In *2013 American Control Conference*, Washington, DC, USA, pp. 3906–3911, 2013.

[16] D. Chu, J. Backstrom, C. Gheorghe, A. Lahouaoula, and C. Chung, "Intelligent closed-loop CD alignment," In *Proceedings of the Control Systems*, Stockholm, Sweden, pp. 161–166, 2010.

[17] R.B. Gopaluni, P.D. Loewen, M.A. Ammar, G.A. Dumont, and M.S. Davies, "Identification of symmetric noncausal processes: Cross-directional response modeling of paper machines," In *Proceedings of the* 45^{th} *IEEE CDC*, San Diego, CA, USA, pp. 6744–6749, 2006.

[18] H. Jansson and H. Hjalmarsson, "Input design via LMIs admitting frequency-wise model specifications in confidence regions," *IEEE Autom. Control*, 50(10):1534–1549, 2005.

[19] W. Rudin, *Principles of Mathematical Analysis*. McGraw-Hill International Edition, 1976.